

First order melting transitions of highly ordered dipalmitoyl phosphatidylcholine gel phase membranes in molecular dynamics simulations with atomistic detail

Thomas Schubert,¹ Emanuel Schneck,^{1,2} and Motomu Tanaka^{1,3,a)}

¹Physical Chemistry of Biosystems, Institute of Physical Chemistry, University of Heidelberg, INF 253, D-69120 Heidelberg, Germany

²Bio Soft Matter Theory, Department of Physics, TU München, D-85748 Garching, Germany

³Cell Biophysics Lab, Institute of Toxicology and Genetics, Karlsruhe Institute of Technology, D-76021 Karlsruhe, Germany

(Received 25 January 2011; accepted 6 July 2011; published online 5 August 2011)

Molecular dynamics simulations with atomistic detail of the gel phase and melting transitions of dipalmitoyl phosphatidylcholine bilayers in water reveal the dependency of many thermodynamic and structural parameters on the initial system ordering. We quantitatively compare different methods to create a gel phase system and we observe that a very high ordering of the gel phase starting system is necessary to observe behavior which reproduces experimental data. We performed heating scans with speeds down to 0.5 K/ns and could observe sharp first order phase transitions. Also, we investigated the transition enthalpy as the natural intrinsic parameter of first order phase transitions, and obtained a quantitative match with experimental values. Furthermore, we performed systematic investigations of the statistical distribution and heating rate dependency of the microscopic phase transition temperature. © 2011 American Institute of Physics. [doi:10.1063/1.3615937]

I. INTRODUCTION

Biological membranes are complex systems vital to all cells. The main structural component of membranes is the lipid bilayer.¹ Similar to other surfactant molecules, lipids suspended in aqueous media are self-assembled into a rich variety of supramolecular architectures that undergo lyotropic and thermotropic phase transitions.^{2–8}

One of the most commonly studied models of biological membranes is that of dipalmitoyl phosphatidylcholine (DPPC). At $T > T_m$, lipid membranes are in the fluid L_α phase, analogous to the smectic A phase of liquid crystals. Notably, the hydrocarbon chains have a high number of *gauche* bonds, retaining a high lateral and rotational mobility. DPPC undergoes a discontinuous phase transition (referred to as the main transition⁹) at $T_m = 41.2^\circ\text{C}$. When the membrane is cooled to $T < T_m$, the hydrocarbon chains of DPPC adopt all-*trans* conformations and form periodically undulating “ripples” (P_β phase).^{10–16} The phase transition enthalpy across the main transition determined by differential scanning calorimetry (DSC) is approximately $\Delta H = 36\text{--}38$ kJ/mol.¹⁷

Further cooling leads to the transition to the planar gel (L_β) phase, where the ordered hydrocarbon chains have even further reduced translational and rotational degrees of freedom. In the case of phosphatidylcholine membranes in the L_β phase, the hydrocarbon chains are tilted by $\sim 32^\circ$ from the membrane normal.^{18–21} This relatively high molecular tilt is caused by the mismatch of the cross-sectional area of the head group and that of hydrocarbon chains (Figure 1). To date, both long-range and short-range order in multi-lamellar lipid

membranes in the gel phase have been extensively characterized by small- and wide-angle x-ray scattering experiments both in isotropic suspensions as well as on planar solid supports.⁵

In order to understand the principles that dominate the hierarchical structural order in biological membranes, various computer simulations have been carried out. Monte Carlo simulations,²² molecular dynamics (MD) simulations,²³ and dissipative particle dynamics methods²⁴ were used to describe lipid membranes with vastly different levels of complexity, ranging from two-dimensional lattice models to all-atom molecular dynamics. For example, Monte Carlo simulations assuming weak leaflet interactions, (e.g., the ten-state lattice model^{25,26}) successfully predicted the main transition enthalpy of DPPC membranes,^{27–29} and described the dynamics of fluid membranes,²² but this approach is not adequate to describe molecular detail. On the other hand, atomic scale molecular dynamics is a powerful tool to gain further insight into molecular/atomic details,³⁰ but this approach cannot currently be used to describe phase transitions due to its high computational cost and thus limited time window. As a compromise, several approaches have been proposed: an implicit solvent effect was used to reduce the number of interacting particles,³¹ and coarse-grained pseudo-atoms enabled one to group the interactions of several atoms.^{32–34} Recently, coarse-grained molecular dynamics simulations have been used to model large-scale structure formation, such as vesicle formation and curvature-induced protein aggregation.^{35,36} More recently, Marrink *et al.* also used a coarse-grained MD to simulate nucleation and cluster growth during the phase transition,³⁷ but their model cannot properly represent the molecular tilt in the gel phase due to the excessively large cross-sectional area of the hydrocarbon chains required in

^{a)} Author to whom correspondence should be addressed. Electronic mail: tanaka@uni-heidelberg.de.

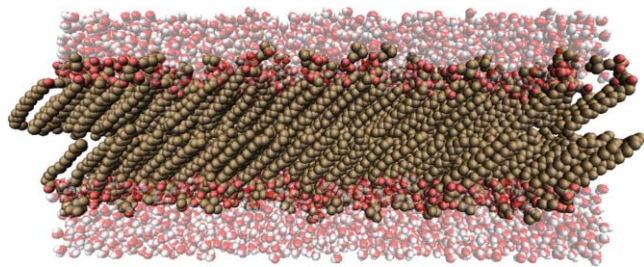


FIG. 1. A gel phase system of 800 DPPC in water. Hydrogen atoms are not shown.

their model. Dissipative particle dynamics^{24,38} based soft potentials can also model spontaneous vesicle formation³⁹ and freezing/melting of gel phase membranes.^{40,41} However, despite the remarkable progress achieved, coarse-grained approaches are not sensitive to molecular detail.

From this viewpoint, all-atom or united-atom MD will likely be able to satisfactorily account for the significant influence of small changes in molecular structures on their phase behaviors found by experiments. Thus, for example, synthetic ether-linked phospholipids form interdigitated gel phases^{42,43} which are not realized by natural ester-linked phospholipids.

For MD simulations, it is necessary to parameterize the force fields and molecular topologies to match experimental results. To date, most of the atomistic MD simulations focused on the fine-tuning of the force fields for lipids in the fluid L_α phase^{44–46} due to the perceived higher biological relevance. However, it should be noted that CHARMM (Ref. 47) force fields previously used for lipids can represent fluid membranes only when the system is expanded by a negative surface tension, thus introducing an arbitrary free parameter. In fact, with these force fields the use of zero surface tension leads to a compact gel phase even beyond the main transition temperature T_m . Only recently Sonne *et al.*⁴⁶ reported a re-parameterization for DPPC based on CHARMM27, and successfully simulated the fluid phase at zero surface tension. In a further recent development, the CHARMM36 potentials appear to enable better area per molecule values with zero surface tension.⁴⁸

Using united-atom force fields, Anezo *et al.*⁴⁹ studied the influence of electrostatics treatment upon membrane simulations and required equilibration times. They reported that 10–20 ns of equilibration time can be necessary even for fluid membrane systems. Importantly, they concluded that many combinations of simulation parameters, electrostatics treatment and force fields can be used to tune the system to a certain area per molecule, which is most often the central criterion for a “correct” simulation of the fluid phase.

On the other hand, there have been fewer reports dealing with the atomistic MD simulations of the lipid gel phase. For the use of a constant volume or area ensemble,⁵⁰ the area per molecule is a prerequisite and most studies have constructed the starting systems based on the structural information obtained by crystallography. Essmann *et al.*⁵¹ used fluid and gel phase lipid membranes in a constant volume ensemble, and simulated the hydration interaction, showing good agreement with the experimentally determined area per molecule, electron density profile, and tilt angle. Tu *et al.*⁵² employed a con-

stant pressure ensemble for short (1 ns) trajectories and calculated spherically and cylindrically integrated reciprocal space maps. Venable *et al.*⁵³ reported further simulations with reasonable agreement with structural parameters determined by experiments. Vries *et al.*⁵⁴ performed temperature jump simulations starting from $T > T_m$ and then equilibrated the system at $T < T_m$. They observed the formation of partially interdigitated structures resembling the ripple phase P_β .⁵⁵

More recently, Leekumjorn and Sum⁵⁶ reported observation of reversible phase transitions for DPPC and dipalmitoyl phosphatidylethanolamine (DPPE) during heating-freezing cycles. The equilibrated gel phase consisted of both ordered and disordered structures, with an area per molecule of 58 \AA^2 that is large compared to experimental findings²¹ ($\sim 48 \text{ \AA}^2$). The calculated phase transition temperature $T_m = 305 \text{ K}$ is lower than the experimental value $T_m = 315 \text{ K}$. This can be attributed to the fast scan speed (2.5 K/ns) leading to a quasi-continuous phase transition.⁹

In the present paper, we propose a new method to simulate the gel phase of lipid membranes with minimum necessary *a priori* knowledge, starting from an easy to generate configuration of 32 lipids. Here, we put the main focus on the chain correlation and ordering of the resulting gel phase membranes, and discuss the effects of the lipid force field and the methodology (system preparation and run parameters) on the resulting structures. Towards this aim, we introduce 3D autocorrelation maps to analyze the ordering of lipid systems. Furthermore, in order to fill the gap in the timescale between experiments and simulations, we study the influence of non-equilibrium thermodynamics on the melting temperature and transition enthalpy.

II. METHODS

A. Simulations

Simulations were performed with the GROMACS software package, version 4 (Ref. 57) (pre-release version 200800503 and version 4.0.3). The OPLS (optimized potentials for liquid simulations) -based united-atom lipid force field and DPPC force field (lipid.itp and dppc.itp) were taken from the literature^{23,44,58–60} and used with the ffgmx force field and TIP3P water. The united-atom model includes non-polar hydrogens in heavy atom sites, while explicitly preserving polar hydrogens. Simulations were run with Berendsen anisotropic pressure coupling, temperature was coupled with the Berendsen thermostat. To reduce calculation time, H-angle restraints and a time-step of 0.004 ps were used.

For the construction of the model gel phase membranes, we made a $4 \times 4 \times 2$ system (32 lipids in a tightly packed bilayer configuration with an area per molecule of 0.40 nm^2) as a starting point. For each monolayer, an energy-minimized upright single lipid was multiplied on a hexagonal lattice with random rotations around the z -axis. This system was then hydrated with GROMACS tools. After the misplaced water molecules were removed, at least 35 water molecules remained for each lipid. This is approximately equal to the equilibrium hydration level for the L_α phase, while 11 water molecules per lipid are observed for the L_β phase. Excess

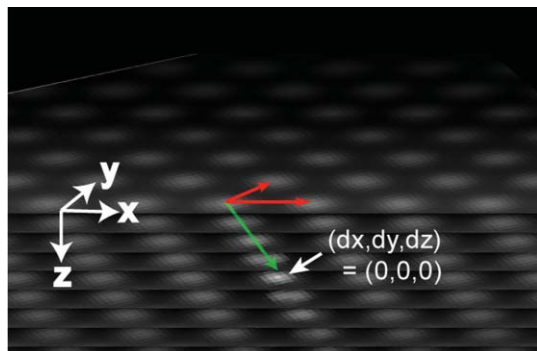


FIG. 2. The 3D-autocorrelation of a highly ordered DPPC membrane monolayer. The red arrows indicate the in-plane vectors of the 2D unit cell while the green arrow indicates the molecular tilt vector. In this representation, the $dz = 0$ plane is in the center of the stack, where each plane is a step of 1 Å. Note that there are no periodicities in the z -direction: the apparent gaps stem from the calculation and display as a stack of xy -planes.

hydration is not expected to have a significant effect on the phase diagram of DPPC.⁶¹

For some special cases, modified topologies were used for initial equilibration of the system as described in main text. In all simulations, 32 lipid molecules were equilibrated for 20 ns at 270 K with the original unmodified force field, and then multiplied 3×3 into 288 lipid systems. These were equilibrated for another 25 ns, and finally evaluated for another 25 ns. Heating scans were performed by single continuous annealing runs, with rates as described in the text.

The runs were performed on HELICS II (IWR, Universität Heidelberg) and the Heidelberg cluster of the bwGRiD initiative. HELICS II uses 4-cpu nodes with AMD quad-core Opterons at 2.8 GHz and 10G Myrinet, while bwGRiD uses 8-cpu nodes with $2 \times$ Intel Xeons at 2.83 GHz and Infiniband interconnects. Systems with 288 lipids could be run at ~ 80 ns/day using 64 cpus. Evaluation of the results was performed with the GROMACS toolset and self-written scripts.

B. 3D autocorrelation

The result of the autocorrelation $C(dx, dy, dz)$ of atomic positions is a 3D map (see Figure 2), which is normalized to unity at the central self-correlation at $(0,0,0)$. For an ordered system with certain characteristic repeat distances the map will exhibit periodic correlation peaks. We calculated the 3D autocorrelation by shifting the coordinate data set by (dx, dy, dz) relative to the original reference coordinates and

measuring the resulting overlap of all atoms using a linear overlap function going to zero at a radius of 0.15 nm. Total overlap for all atoms are summed for each (dx, dy, dz) to give the 3D map. The maps are normalized to unity at the self-correlation peak at $(0,0,0)$. In order to reduce calculation time, the software was written in “C” using the message passing interface (MPI) framework and was run on large compute clusters using several hundred central processing units (CPUs). The autocorrelation maps of individual membrane leaflets were calculated separately.

For evaluation of the unit cell from a map, one determines the in-plane vectors (at $dz = 0$) from the self-correlation peak to two linearly independent first-order peaks which fully describe the 2D unit cell (see Figure 2). Exact peak positions are determined from 2D-Gaussian fits to the peaks. The molecular tilt vector is determined by the tilt angle and the tilt direction in the xy -plane projection (relative to the 2D unit cell). Both aspects are extracted from 2D-Gaussian fits to the self-correlation peak at different dz .

The existence of lateral long-range (far) ordering of the lipid chains is a major discriminating parameter between solid and melted membrane phases. The autocorrelation $C(dx, dy, dz)$ of a system is a straightforward way to access the “order” or “disorder” of hydrocarbon chains in a defined manner. For the quantitative evaluation of the calculated 3D autocorrelations, we introduced two new order coefficients, O_{iso} and O_{far} (Figure 3).

O_{iso} represents the rotational (an)isotropy in the 2D autocorrelation map at $dz = 0$ (not to be confused with the coordinate z). It is defined as the maximum amplitude difference over a full rotation of this plane of zero z -displacement (where correlation intensity is maximal):

$$O_{iso} = \max(C_{rot}(\varphi)) - \min(C_{rot}(\varphi)), \quad \text{with}$$

$$C_{rot}(\varphi) = \frac{1}{\pi R} \int_0^R \int_0^{2\pi} C_{dz=0}(r, \varphi') rot(C_{dz=0}(r, \varphi'), \varphi) d\varphi' dr.$$

Here, $C_{dz=0}(r, \varphi')$ denotes the autocorrelation function $C(dx, dy, dz)$ at $dz = 0$ in polar coordinates, and $rot(f, \varphi)$ the rotation of a function f by an angle φ . As the effect is most prominent in the first order the calculation is restricted in this study to within a radius of $R = 0.85$ nm. In practice, O_{iso} is calculated by rotating the map stepwise through 360° , while multiplying with the original reference map, summing over all pixels within the radius R and normalizing to the number of pixels. For a highly ordered system, changes in the pixel

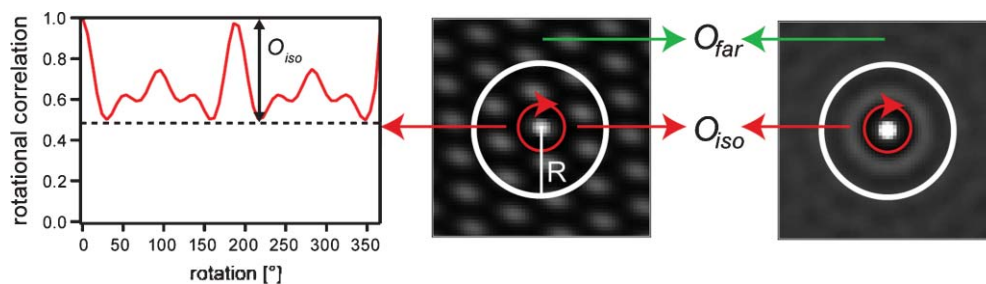


FIG. 3. Illustration of the new order coefficients O_{far} and O_{iso} for a highly ordered and an isotropic melted system.

intensity during the rotation (alternation of peak and valley overlaps) result in an oscillating rotation-correlation function (Figure 3) with a high O_{iso} value, whereas the isotropic map of a disordered system results in a smooth curve with constant amplitude and a low O_{iso} . However, O_{iso} does not measure the “near order,” it is rather an aspect of the total system order. To illustrate, even in a disordered phase an isotropic near ordering is present (the homogeneous ring in Figure 3, right), but O_{iso} becomes zero.

On the other hand, the coefficient O_{far} is a direct measure of long-range ordering. We define O_{far} as the standard deviation of the xy -plane at $dz = 0$ at a distance larger than R , reflecting the “spikiness” of the autocorrelation map outside the first order. For an ordered system with many sharp correlation and anti-correlation peaks the standard deviation is high and thus O_{far} is large. A fully disordered system will have a uniform gray level in the autocorrelation with no spikes, so that the standard deviation and thus O_{far} will be equal to zero.

Due to the relevance for the gel phase, in the following discussion of ordering we use the autocorrelation of all carbon chain atoms but no glycerol or head group atoms, except where noted otherwise.

III. RESULTS AND DISCUSSION

A. Structural and ordering aspects

1. Introducing new ways to construct gel phase systems

As a first step, we investigated ways to obtain equilibrated gel phase system. As mentioned above, our main goal was that our membrane gel phase systems should represent experimental results while using as little *a priori* information as possible, in order to establish methods for tackling systems less well known than DPPC. Previously, the best ordering had been achieved by constructing membranes using crystallographic information, which however is in contrast to our demand for little *a priori* information. Furthermore, in this work we highlight some drawbacks of creating a gel phase system by simple cooling/freezing.

Instead, we introduce two “assisted freezing” approaches, which effectively bypass a nucleation stage and significantly accelerate equilibration to high ordering compared to the method of “natural freezing”. We will show that we can obtain highly ordered systems which match many known experimental parameters. In order to monitor the system development over a large temperature scan range, we chose 270 K as the starting temperature and we compare three different starting systems for this condition. In Sec. III A 2, we will also discuss a system constructed and equilibrated at 300 K.

The presented methods are (1) initially fixing the chain dihedrals in all-*trans* configurations, (2) using a lipid force field that has an intrinsic tendency towards a gel phase, and (3) simply cooling the system, starting from a melted configuration. All the three methods start with randomly rotated upright lipids in a 4×4 bilayer block (32 lipids, see also Sec. II). We consider the bias in methods (1) and (2) smaller

than in an explicit construction, so that one might consider them as “assisted freezing,” while (3) is “natural freezing.”

The presented strategies are

Method (1): All chain dihedrals are temporarily fixed in their *trans* positions by exchanging them for improper (non-rotating) dihedrals. Temporarily fixing the chain dihedrals reduces the conformational space the lipid molecules have to sample in order to find a packing minimum, which is expected to reduce the necessary equilibration times. In practice, equilibrating with fixed dihedrals leads to very compact systems, which remain highly ordered upon exchange for the unmodified lipid force field with normal chain dihedrals.

Method (2): One starts with a special force field that exhibits a tendency to form compact ordered systems due to a severely mismatched attraction/repulsion balance. A DPPC force field generated by PRODRG (Ref. 62) tends towards this behavior, as do pre-2010 versions of the CHARMM force field.^{46,48} We used a PRODRG-generated force field further modified by removing all partial charges. The removal of partial charges leads to even more compact systems, but reintroduction of charges has to be done stepwise in multiple short equilibration steps to avoid system explosion. The system is then equilibrated with the unmodified lipid force field.

Method (3): The starting block is created using the unmodified force field by slowly cooling a melted system of 32 lipids over 600 ns at 0.1 K/ns from 330 K to 270 K. The system was thus kept for ~ 450 ns at temperatures below the expected melting temperature for DPPC of $T_m = 315$ K.

As described in Sec. II, the 4×4 starting blocks were multiplied into the desired final system size, and equilibrated with the correct standard force field. In the following, the 288-lipid starting systems created by these methods at 270 K are denoted by system (1), system (2), and system (3), respectively, and are shown in Fig. 4. The results shown are typical and representative, though naturally there is a certain random component due to the random starting configurations. A visual inspection of these systems shows a clear trend: system (1) has the highest ordering, followed by system (2) and last system (3). The differences in ordering between the systems can be quantified, as summarized in Table I.

System (1) is nearly all-*trans* with 0.7 *gauche*/chain. For system (2), one sees an overall higher level of *gauche* rotamers with 1.1 *gauche*/chain, while system (3) is very disordered with 2.1 *gauche*/chain, which is close to the value of 3.3 *gauche*/chain we observe for a melted system. Experimentally, values of 1.0 *gauche*/chain or less are observed.^{9,64,65} We also looked at the fraction of *gauche* depending on the position of the bond in the carbon chains, see Fig. 5. For system (1), a clear maximum of *gauche* is observed at the start of the *sn2* chain, matching experimental results.⁶⁶⁻⁶⁸

Quite striking is that the chain tilt angle appears to be correlated with the system order/disorder. Analysis shows that in system (2), the chain tilt is 32° (apparently matching experiments), but we can see that the better ordered system (1) has a value of 45° . System (3) is weakly ordered and shows a very small average molecular tilt. The area per molecule is 0.55 nm^2 , 0.52 nm^2 , and 0.52 nm^2 for systems (1), (2), and (3), respectively. However, the area per molecule and the chain tilt are interdependent factors. Not surprisingly, the

TABLE I. Selected structural and ordering parameters for different systems of 288 DPPC.

	Area per molecule	Tilt	Thickness (D_{HH})	Volume per lipid	<i>gauche</i> / chain	O_{iso}	$O_{far} [\times 10^2]$
270 K, method (1)	0.55 nm ²	45°	3.81 nm	1.098 nm ³	0.71	2.0	10.7
270 K, method (2)	0.52 nm ²	32°	4.17 nm	1.144 nm ³	1.14	0.71	3.4
270 K, method (3)	0.52 nm ²	4°	4.36 nm	1.158 nm ³	2.11	0.12	1.4
300 K, method (1)	0.50 nm ²	37°	3.88 nm	1.228 nm ³	0.94	1.4	7.5
330 K, fluid	0.68-0.69 nm ²	0°	3.74 nm	1.122 nm ³	3.30	0.02	0.5
300 K, experimental	0.48 nm ² ^a	31.6° ^a	4.28 nm ^a	1.15 nm ³ ^b	<1 ^c
323 K, experimental	0.63 nm ² ^d	0°	3.80 nm ^d	1.229 nm ³ ^d	~3.8 ^e

^aReference 21.^bReference 7.^cReference 9.^dReference 63.^eReference 64.

membrane thickness also correlates strongly with the tilt angle, in addition to chain disordering which contributes to reduced membrane thickness accompanied by an increased area per molecule. The azimuthal correlation between the chain tilts in the two membrane leaflets was found to be essentially parallel whenever there was a significant tilt. This parallel orientation between the leaflets did not drift during simulation runs. The volume per lipid, calculated by subtracting the volume occupied by the water molecules from the simulation volume, was found to be in acceptable agreement with experiments, see Table I. Understandably, factors indicating greater ordering (order parameters, fraction of *gauche*) correlate with

reduced average lipid volume. Furthermore, we could confirm for all systems that we have a gel phase with chain correlation but no headgroup correlation,⁶⁹ as shown in Fig. 6.

A first conclusion is that creating a gel phase starting system by freezing a small building block is very unlikely to yield useful results without extremely long equilibration. It might be conceivable that freezing a larger system than 32 lipids can lead to better partial ordering due to facilitated nucleation, but this is beyond the scope of this work. A second important observation is that disorder correlates with a reduced average chain tilt angle. In this light, we conclude that the equilibrium tilt angles determined by the force field only become visible in a highly ordered gel phase system and the effect of the force field on gel phase structures should only be judged from such systems. Furthermore, one might have to consider system size effects^{58,70} and influence of metastability (slow equilibration) of the starting system configuration. The method of using initially fixed chain dihedrals produces highly ordered gel phase systems in a simple fashion. Notably, systems created at lower temperature achieve a higher level of ordering. The deviations from the experimental values should be determined mainly by the force field if sufficiently good chain ordering is achieved during construction of the system. But overall, we find that we can construct systems that represent DPPC gel phase membranes well enough to obtain melting transitions with convincing properties (see below).

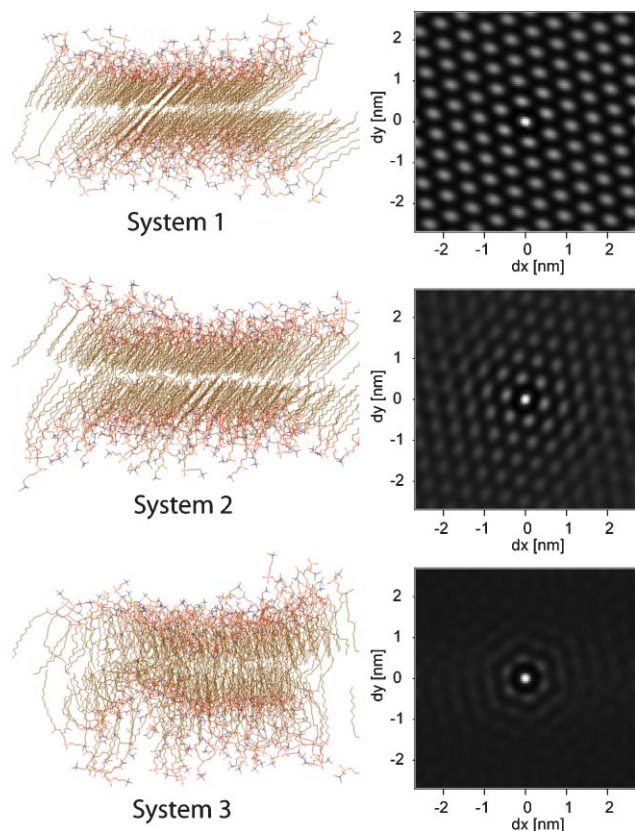


FIG. 4. The three systems with 288 DPPC used to compare the gel phase construction methods and their corresponding autocorrelation maps (of a single leaflet).

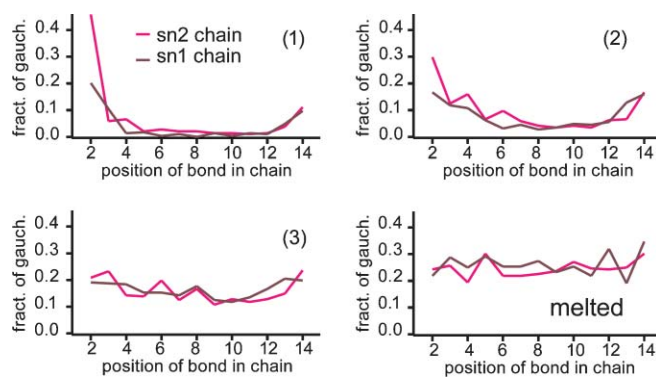


FIG. 5. Comparison of the distribution of *gauche* rotated bonds along the lipid chains for systems (1), (2), and (3) at 270 K and a melted system at 330 K. These graphs were extracted from the final frame (snapshot) after equilibrating.

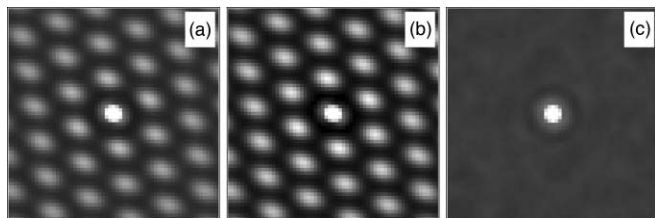


FIG. 6. Autocorrelation of system (1) with different atom subsets: (A) All lipid atoms. (B) Chain carbons. (C) All lipid atoms except chain carbons. The other systems show similar results.

2. DPPC unit cell and chain tilt at 270 K and 300 K

One of the most prominent advantages that 3D autocorrelation can offer is that it becomes possible to compare the simulation unit cell to experimental unit cell parameters obtained with high accuracy from scattering experiments such as wide angle x-ray scattering.²¹ The 3D-autocorrelation maps (calculated for each monolayer separately) include the full information about the unit cell as well as the molecular tilt in the membrane plane (see Figs. 2 and 7). It is in contrast to previous approaches, where the evaluations were not based on the basic unit cell.^{52,54,71,72}

In order to avoid extremely long equilibration times in the gel phase system after temperature changes, another system was constructed and equilibrated directly at 300 K. The structural details for the system at 300 K are included in Table I. Figure 7 shows the autocorrelation maps at $T = 270$ K (left) and 300 K (right) at $dz = 0$. As shown in figure, the distortion was more prominent at 270 K than at 300 K. A chain tilt of $\Theta = 45^\circ$ was observed at 270 K, while a tilt of $\Theta = 37^\circ$ was observed at 300 K. The area per molecule in the system constructed at 300 K was 0.50 nm^2 , which is smaller than the value of 0.55 nm^2 we obtained from a construction at 270 K discussed above. These areas can be correlated with the difference in the tilt angles and degree of ordering. Importantly, the smaller area at higher temperature appears contrary to experimental results which report a positive area expansion coefficient. However, during heating scans of a single system (see below), a positive area expansion coefficient is indeed observed as well as a reasonable value for $d\Theta/dT$. Here,

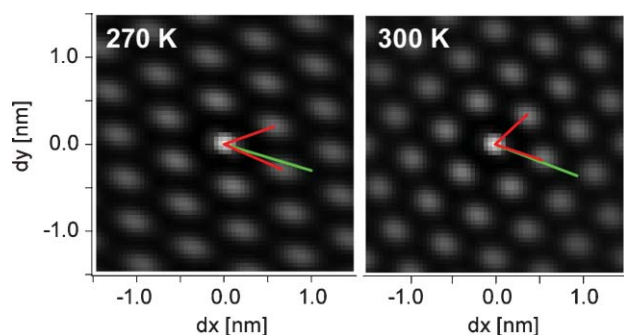


FIG. 7. Unit cells at $dz = 0$ calculated from 3D autocorrelation of two systems of 288 DPPC, at 270 K (left) and 300 K (right), independently constructed with method (1). Red lines indicate in-plane unit cell vectors while the green line indicates the tilt vector projection (comparison to Figure 2). At 300 K, the chains are tilted towards the nearest-neighbor at 37° , compared to 45° at 270 K. The increased tilt leads to a strong unit cell distortion.

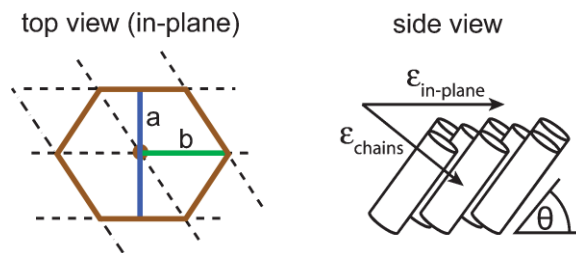


FIG. 8. Left: Sketch of the orthorhombic in-plane 2D unit cell vectors a and b . They are suitable for describing an ordered lipid system with a molecular tilt in direction of b (nearest-neighbor tilt), which induces a stretching distortion in direction of b . Right: Such a distortion can be described with the in-plane distortion parameter ϵ . Also, a distortion perpendicular to the tilted chains (due to deviations from the cylindrical model) can occur, denoted by ϵ_{chain} .

we consider the discrepancy in areas of separately constructed systems to be a metastability issue due to different levels of ordering achieved initially during construction. Our findings could be consistent with the effective headgroup size determined by the force field being too large.

In general, a chain tilt induces a distortion of the hexagonal lattice. As presented in Fig. 7, the unit cell chain tilt is approximately towards the nearest neighbor. Thus, the unit cell can be approximated as an orthorhombic lattice with two-fold symmetry. Figure 8 illustrates the in-plane unit cell vectors a and b , where stretching occurs in direction of b .

In the simulations we observed slightly oblique unit cells with imperfect nearest-neighbor tilt (Figure 7) and thus three-fold symmetry. We consider such deviations from an orthorhombic unit cell a metastability issue of the simulations.⁵² Thus, we used the average plane spacings d_{20} and $d_{11} = (d_{1,+1} + d_{1,-1})/2$ (Ref. 73) to calculate the orthorhombic unit cell vectors a and b :¹⁹

$$a = 2d_{20} \quad \text{and} \quad b = \frac{d_{11}}{\sqrt{1 - (d_{11}/d_{20})^2}}. \quad (1)$$

At 300 K, we find the in-plane orthorhombic vectors $a = 8.36 \text{ \AA}$ and $b = 5.85 \text{ \AA}$, and at 270 K, $a = 8.18 \text{ \AA}$ and $b = 6.65 \text{ \AA}$. For DPPC at 24°C , Sun *et al.*¹⁹ reported in-plane orthorhombic unit cell vectors of $a = (8.488 \pm 0.0008) \text{ \AA}$ and $b = (5.64 \pm 0.02) \text{ \AA}$. From the small differences seen for the vector a (perpendicular to the tilt) it appears that in the simulations the chains pack slightly more densely than seen in experiment. The larger values of b seen in the simulations are consistent with the larger tilt angles.

From the orthorhombic unit cell vectors one can calculate the distortions ϵ and ϵ_{chain} as^{21,74}

$$\epsilon = 1 - \frac{a}{\sqrt{3}b} \quad \text{and} \quad \epsilon_{chain} = 1 - \frac{a}{\sqrt{3}b \cos \Theta}, \quad (2)$$

where ϵ is the in-plane stretching distortion in direction of the vector b , ϵ_{chain} is the distortion perpendicular to the chains, and Θ is the chain tilt (Figure 8). An orthorhombic stretching induced by a nearest-neighbor tilt leads to a positive sign for ϵ . For an undistorted hexagonal lattice, $a = \sqrt{3}b$ and $\epsilon = 0$. On the other hand, the molecular shape from an ideal cylinder determines ϵ_{chain} .

We found that the in-plane distortion ε at $T = 270$ K, $\varepsilon(270 \text{ K}) = +0.291$, is much larger than that at 300 K, $\varepsilon(300 \text{ K}) = +0.175$. In fact, the distortion calculated for $T = 300$ K agrees well with the corresponding value calculated from the experimental result at $T = 297$ K, $\varepsilon(297^\circ\text{C}) = +0.131$ (Sun *et al.*¹⁹). Interestingly, the distortion perpendicular to the chain was not influenced by the temperature, $\varepsilon_{\text{chain}}(300 \text{ K}, 270 \text{ K}) \sim -0.03$. This value is also in excellent agreement with the experimental value reported by Sun *et al.*, $\varepsilon_{\text{chain}}(298^\circ\text{C}) \sim -0.03$. The obtained results confirmed that the force field of lipid molecules we used in our simulations well represents the shape of lipid molecules.

Finally, the chain tilt can in general be correlated to the ratio between the cross-sectional areas of the headgroups and chains:

$$\cos \Theta = \frac{2 \times A_c}{A_H}, \quad (3)$$

where Θ is the chain tilt relative to the membrane normal, A_c is the cross-sectional area of a single chain and A_H is the cross-sectional area of the headgroups. The area per chain can be calculated from

$$A_c = \frac{ab \cos \Theta}{2}, \quad (4)$$

where Θ is the molecular tilt angle. In the simulations, we find $A_c(300 \text{ K}) = 19.5 \text{ \AA}^2$ and $A_c(270 \text{ K}) = 19.2 \text{ \AA}^2$. It should be noted that these values are in excellent agreement with the experimental values,²¹ $A_c(300 \text{ K}) \sim 20.1 \text{ \AA}^2$ and $A_c(270 \text{ K}) \sim 19.6 \text{ \AA}^2$.

Although some of the differences observed between the membranes at 270 K and 300 K suggest that much longer simulation times would be appropriate for membranes in the gel phase to reach full equilibrium, the gel phase model created here is capable of representing many structural parameters obtained by experiments.

B. Melting transitions

1. Phase transition enthalpy

To monitor the thermotropic phase transition of lipid membranes, we performed heating scans of the gel phase systems, which is analogous to DSC experiments (see also supplemental information⁸³). Figure 9 represents the total energy for a heating scan of system (1) with 0.5 K/ns, exhibiting a jump at 321 K. This discontinuous jump can be interpreted in terms of the phase transition enthalpy,^{9,75-77} since the contribution from the pressure and volume terms are negligibly small. Along with the transition, a loss of chain ordering is observed. Although the heating scan rate is too fast to keep the system near the thermodynamic equilibrium, the transition temperature obtained in the simulation is close to the experimental main transition temperature of DPPC membranes, $T = 314.5$ K.

To extract the phase transition enthalpy, one can take two different approaches. In the first approach, the total energy curve (black line in Fig. 9(a)) was directly fitted with a sigmoidal function together with two independent linear components (red line in Fig. 9(a)), and the derivative of the fit

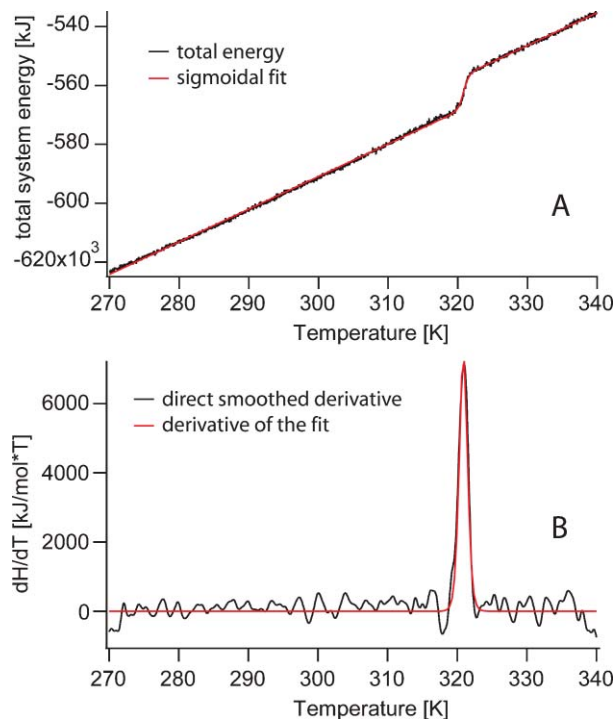


FIG. 9. Total energy over temperature for a heating scan with 0.5 K/ns with system (1). (A) The total system energy (black) and the sigmoidal fit (red). (B) The derivative of the smoothed total energy (black), and the derivative of the sigmoidal fit (red).

curve (red curve in Fig. 9(b)) was plotted versus temperature. Alternatively, the total energy curve can be smoothed, and its derivative plotted directly as an analogue of a DSC scan (black in Fig. 9(b)). After subtraction of constant offsets, the curves obtained by the two approaches showed good quantitative agreement.

Although the curves presented in Fig. 9(b) look similar to experimental DSC scans,⁸⁰ it should be noted that the peak width of such a microscopic transition (FWHM = 1.5 K) is different from the one in a macroscopic heat capacity scan. The former is a melting event in a single unit system, which is instantaneous and broadened due to limited equilibration at fast heating rates. On the other hand, the latter has been described by the equilibrium occupation of two states by an ensemble of cooperative units.

To highlight the influence of the initial gel phase on the phase transition, the simulated heat capacity scans for system (1) and (2) are compared in Fig. 10. Here, the heating rate was set to be 1 K/ns for both simulations for practical convenience. The simulated heat capacity scan of the ordered system (1) shows a sharp peak at around 320 K (blue curve), which is comparable to that observed at the heating rate of 0.5 K/ns (Fig. 9(b)). On the other hand, the heat capacity scan of the less ordered system (2) exhibited a broad transition peak around 305 K (Figure 10, red curve), which is about 10 K lower than the experimental value. It is remarkable that the position and the width of the broad transition peak observed for the system (2) are almost identical to the transition previously simulated by Leekumjorn and Sum⁵⁶ who used a very similar modeling approach but with weakly ordered systems.

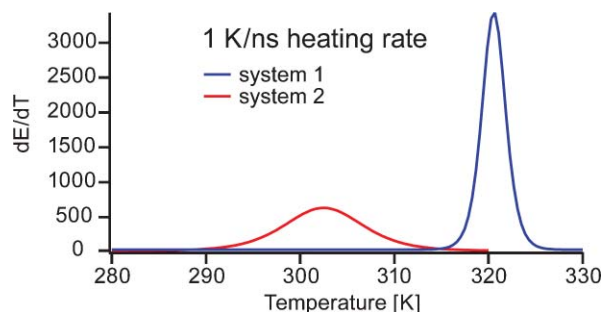


FIG. 10. Comparison of heat capacity scans for systems (1) and (2), simulated at a heating rate of 1 K/ns. System (2) shows a broad transition peak at around 305 K, while system (1) shows a sharp transition near 320 K.

From the simulated heat capacity scans, the phase transition enthalpy was calculated by normalization with the number of DPPC molecules. We obtained an enthalpy of $\Delta H = 40$ kJ/mol for the highly ordered system (1), but only $\Delta H = 24$ kJ/mol for the less ordered system (2). The corresponding scans are shown in Fig. 10. It should be noted that the values were taken from scans where we did not observe distinct pre-transitions. The calculated transition enthalpy matches previously reported values for the DPPC, $\Delta H = 36\text{--}38$ kJ/mol,^{17,78,79} as well as the value from our reference measurements, $\Delta H = 39.7$ kJ/mol (see supplemental information⁸³). In contrast to systems (1) and (2), the heat capacity scan of the poorly ordered system (3) showed no detectable phase transition. These findings strongly suggest that the choice of the gel phase is crucial to adequately simulate the thermotropic phase transition. We concluded that the highly ordered system (1) is closer to the global minimum conformation in the gel phase (as determined by the force field used). In Secs. III B 2–III B 3, we will focus on the system (1) in detailed description of the molecular structures through the transition.

2. Changes in structural parameters during the transition

Beyond enthalpic considerations, we further looked at some structural parameters during heating scans, such as area per molecule, the fraction of *gauche*, the chain tilt angle, and our new order coefficients O_{far} and O_{iso} . Note that the chain tilt was extracted from the 3D-autocorrelation maps (Fig. 11). This definition yields the same information that can be determined experimentally in diffraction experiments and avoids assigning the molecular axis between arbitrary atoms.

Figure 12 represents the development of the structural parameters during a heat scan at 0.5 K/ns. The area per molecule and the fraction of *gauche* slowly increase at temperatures below T_m . Both order coefficients O_{far} and O_{iso} show a clear decrease in the correlation below the phase transition and undergo an abrupt complete loss of order at T_m . Especially the isotropy O_{iso} shows the clearest contrast to the fluid phase.

On the other hand, the molecular tilt angle remains almost unchanged until the melting transition. At $T < T_m$, changes in the tilt angle according to the increase in temperature is approximately $(d\Theta/dT) \sim -0.06^\circ/\text{K}$, which is con-

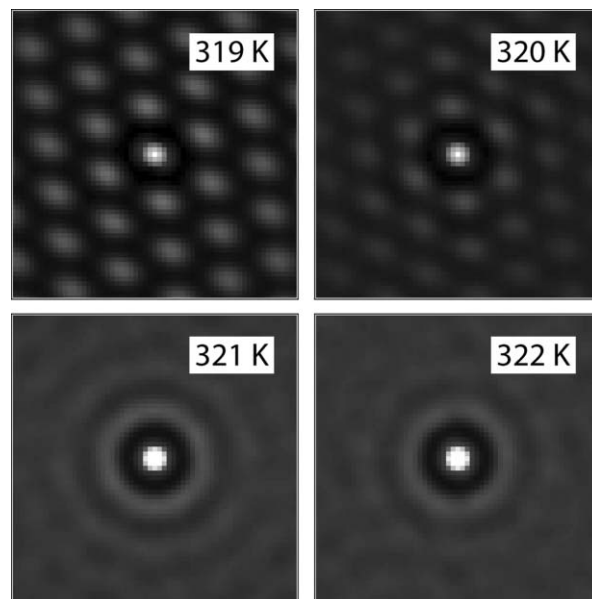


FIG. 11. Autocorrelation of the chain carbon atoms of the top monolayer of system (1) during melting, at 0.5 K/ns. The intensity of the two lower images is scaled by a factor of two.

sistent with the experimentally determined values, $(d\Theta/dT) \sim -0.10^\circ/\text{K}$ by Sun *et al.*²¹ Taking the increase in the area per molecule with temperature $(dA/dT) = 3.5 \times 10^{-4} \text{ \AA}^2 \text{ K}^{-1}$, we could calculate the lateral thermal expansion coefficient $\alpha_A = (dA/dT)/A = 6 \times 10^{-4} \text{ K}^{-1}$. This is in acceptable agreement with the experimental value $\alpha_A = 2 \times 10^{-4} \text{ K}^{-1}$ reported by Sun *et al.*²¹ Furthermore, the tilt angle reached by heating the system up to 300 K was higher than the one in the system constructed at 300 K, confirming that membranes in the gel phase need longer times than used here to reach full equilibrium.

The area per molecule reached in the fluid phase around 330 K was around $0.68\text{--}0.69 \text{ nm}^2$, which is slightly larger than the best current experimental value of 0.63 nm^2 by

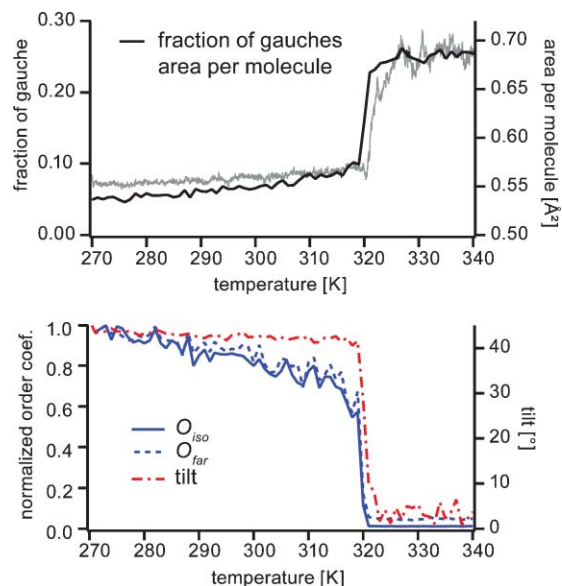


FIG. 12. Changes in molecular structural parameters in system (1) during the heating scans at 0.5 K/ns.

Kucerka *et al.*⁶³ In future studies the response of such deviations of the discussed structural parameters from the experimental values to changes in the lipid force field could be used as a basis for a systematic force field optimization.

One of the remarkable findings is that the structural parameters exhibit different time responses to the heating. For example, the fraction of *gauche* as well as O_{iso} and O_{far} undergo transitions $\sim 1\text{K} = 2\text{ ns}$ before changes in the area per molecule and tilt angle take place. This finding seems reasonable if parameters related to entropy (and thus ordering) play a dominant role in the transition. Thus, it is plausible to assume that the time difference of 2 ns coincides with the intrinsic relaxation time of the system, which will significantly depend on the system size and simulation parameters. Last but not least, the fact that the phase transition of the entire membrane occurs quasi-instantaneously suggests that the transition in our simulation is an event within a single cooperative unit.

Interestingly, in some of the simulation runs with the less ordered system (2) at heating rates of 0.5 K/ns formation of structures resembling the ripple phase were observed.⁵⁵ Such ripple formation was observed with system sizes of 288 lipids as well as with system size increased to 800 lipids in a box size of $\sim 13\text{ nm}$ (corresponding to the experimentally observed length scale of a single ripple wave). These preliminary observations motivate further studies which lie beyond the scope of the current work.

3. Influence of the heating rate on T_m

To gain deeper insights into the influence of the heating rate on the microscopic T_m , we performed multiple runs at scan rates of $r = 5\text{ K/ns}$, 2 K/ns , 1 K/ns , and 0.5 K/ns . As

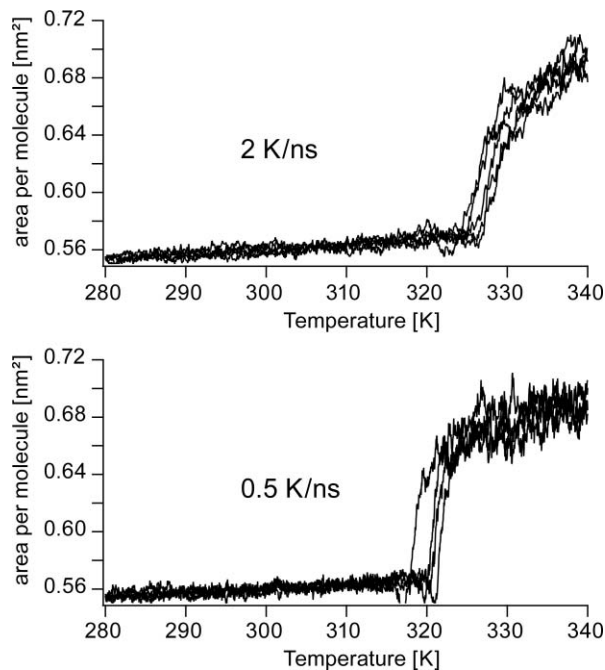


FIG. 13. Area per molecule of heating scans for system (1) displaying melting events. We find a distribution of the microscopic T_m and a scan rate dependency.

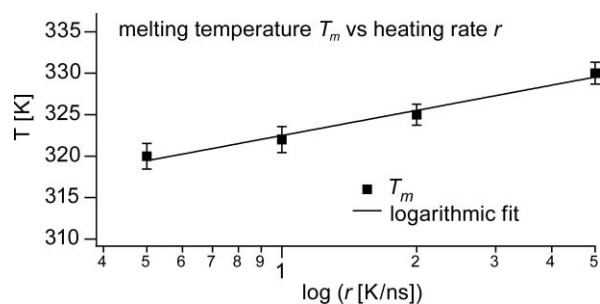


FIG. 14. Dependency of the average melting temperature on the heating rate. The error bars are the standard deviations. The solid line is a linear fit in the half-logarithmic plot, as discussed in the text.

presented in Fig. 13, we observed a clear dependence of T_m on the heating rate. We defined the melting temperature T_m for a single transition event at the onset of the transition, which excludes most effects of slow box equilibration. Refreezing events were not observed.

As shown in Fig. 14, the transition temperature T_m showed a distinct increase ($\Delta T_m \sim 5\text{ K}$) according to the increase in the heating rate from 0.5 K/ns to 2 K/ns. In Fig. 14, the average microscopic melting transition temperature as well as its standard deviation are plotted versus the logarithm of the heating rates. Empirically, we found that in this regime of scan rates T_m is proportional to the logarithm of heating rate in this regime. It should be noted that the situation is mathematically analogous to the dependence of the average rupture force on the pulling velocity in irreversible bond rupture events.^{80–82}

A further decrease in the heating rate should finally lead to the equilibrium T_m as determined by the molecular force field. Here, the functional dependency must of course deviate from a logarithm. Since the simulations (down to 0.5 K/ns) presented here provide an upper limit ($T_m = 320\text{ K}$), it is plausible to expect that the value defined by the lipid force field would further approach to the experimental value of 314.5 K.

The statistics of T_m was evaluated by extracting T_m from a total of 15 runs at a constant heating rate of 0.5 K/ns, yielding a standard deviation of $\sim 1.5\text{ K}$ (FWHM $\sim 3.5\text{ K}$) around 320 K. It is important to note that the statistical distribution of T_m calculated here is a property determined far from equilibrium, and thus it is not directly related to the peak widths ($\sim 0.2\text{ K}$ FWHM) obtained from DSC experiments,⁹ which are performed at much slower heating rates.

IV. CONCLUSIONS

Molecular dynamics simulation studies of lipid membranes in the gel phase are still rare, especially on the atomistic detail level. In this study, we have explored new methods to create and analyze lipid gel phase systems using the experimentally and theoretically well-studied lipid DPPC. We investigated gel phase membranes created by three different approaches with minimum required *a priori* knowledge of the crystallographic details. We find that the apparently “natural” approach of cooling a melted system results in a highly disordered solid phase when equilibrating in a timeframe currently

accessible in MD simulation. Instead, initially fixing the chain dihedrals in an all-*trans* configuration is the most promising way to easily create a highly ordered gel phase membrane. This method might be described as “assisted freezing” and should introduce only a minimal amount of bias. The success of our approach is shown by the formation of highly ordered gel phase systems with a molecular tilt angle (37°) and area per molecule (0.50 nm^2) that were compared to the experimentally reported values (32° and 0.48 nm^2 , respectively). Furthermore, we could show that the average molecular tilt angle correlates with the ordering of the membrane system. According to our findings, disorder reduces the average tilt. Moreover, the molecular tilt appears metastable during heating, so that any conclusions about the equilibrium structure predicted by a certain force field for the gel phase must be reviewed very critically with respect to structural metastability and thermal history. We find that the influence of the system ordering will likely mask the influence of the force field for many features in the gel phase.

As a major methodological improvement, we introduced 3D autocorrelation of the system as a way to gain complete information over the unit cell as well as system ordering. The knowledge of the unit cell vectors allows comparison with results from diffraction experiments. Moreover, we introduce useful ways to quantify long and short range ordering from autocorrelation maps.

In a second line of investigation, we looked at melting transitions. For the first time in MD simulations with atomistic detail we observed sharp first order melting transitions. In general, we observed a dependency of the melting transition features on the initial system ordering. The appearance of discontinuous well-defined melting transitions correlated with high system ordering. We show that it is possible to quantitatively analyze the energy changes involved in melting. Upon melting we observed a very distinct discontinuous increase in the total system energy which we identify as the transition enthalpy. In fact, we could show that a highly ordered system exhibits a phase transition enthalpy ($\sim 40 \text{ kJ/mol}$) close to the experimental value. In more detailed investigations, we observed a statistical distribution of melting events and a heating rate dependency of the average melting temperature pointing towards an equilibrium phase transition temperature T_m below 320 K and close to the experimental T_m of DPPC at 314.5 K . Such thermodynamic considerations have been completely lacking in the literature so far, and further work in this direction should enhance our understanding of lipid models.

The observations made using our novel structural and thermodynamic approach might open new ways to advance our understanding of lipid membrane simulations in general and could help improve current lipid models. Importantly, the results we presented give confidence to extend such simulations to less well known systems where no detailed manual system construction is possible.

ACKNOWLEDGMENTS

We would like to thank Professor David Pink for insightful comments during manuscript preparation, and Dr. Berk Hess (MPI für Polymerforschung, Mainz) for helpful

discussions. We are grateful for computing time on the Heidelberg clusters HELICS II (University of Heidelberg) and bwGRiD (<http://www.bw-grid.de>, member of the German D-Grid initiative). E.S. thanks the State Baden–Württemberg for the fellowship.

- ¹S. J. Singer and G. L. Nicolson, *Science* **175**, 720 (1972).
- ²E. Sackmann, *Science* **271**(5245), 43 (1996).
- ³E. Sackmann and M. Tanaka, *Trends Biotechnol.* **18**, 58 (2000).
- ⁴M. Tanaka and E. Sackmann, *Nature (London)* **437**(7059), 656 (2005).
- ⁵J. F. Nagle and S. Tristram-Nagle, *Biochim. Biophys. Acta* **1469**(3), 159 (2000).
- ⁶R. P. Rand and V. A. Parsegian, *Biochim. Biophys. Acta* **988**(3), 351 (1989).
- ⁷S. Tristram-Nagle and J. F. Nagle, *Chem. Phys. Lipids* **127**(1), 3 (2004).
- ⁸*Lipid Bilayers: Structure and Interactions*, edited by T. Gutberlet and J. Katsaras (Springer-Verlag, Berlin, 2001).
- ⁹D. Marsh, *Chem. Phys. Lipids* **57**(2–3), 109 (1991).
- ¹⁰G. Cevc, *Biochim. Biophys. Acta* **1062**(1), 59 (1991).
- ¹¹B. A. Cunningham, A.-D. Brown, D. H. Wolfe, W. P. Williams, and A. Brain, *Phys. Rev. E* **58**(3), 3662 (1998).
- ¹²J. Katsaras, S. Tristram-Nagle, Y. Liu, R. L. Headrick, E. Fontes, P. C. Mason, and J. F. Nagle, *Biophys. J.* **78**(1), 20a (2000).
- ¹³K. Sengupta, V. A. Raghunathan, and J. Katsaras, *Phys. Rev. E* **68**(3) (2003).
- ¹⁴W. J. Sun, S. Tristram-Nagle, R. M. Suter, and J. F. Nagle, *Proc. Natl. Acad. Sci. U.S.A.* **93**(14), 7008 (1996).
- ¹⁵T. Kaasgaard, C. Leidy, J. H. Crowe, O. G. Mouritsen, and K. Jorgensen, *Biophys. J.* **85**(1), 350 (2003).
- ¹⁶R. Krbecek, C. Gebhardt, H. Gruler, and E. Sackmann, *Biochim. Biophys. Acta* **554**(1), 1 (1979).
- ¹⁷S. Mabrey and J. M. Sturtevant, *Proc. Natl. Acad. Sci. U.S.A.* **73**(11), 3862 (1976).
- ¹⁸S. Tristram-Nagle, R. Zhang, R. M. Suter, C. R. Worthington, W. J. Sun, and J. F. Nagle, *Biophys. J.* **64**(4), 1097 (1993).
- ¹⁹W. J. Sun, R. M. Suter, M. A. Knewton, C. R. Worthington, S. Tristram-Nagle, R. Zhang, and J. F. Nagle, *Phys. Rev. E* **49**(5), 4665 (1994).
- ²⁰J. Katsaras, D. S. C. Yang, and R. M. Epand, *Biophys. J.* **63**(4), 1170 (1992).
- ²¹W. J. Sun, S. Tristram-Nagle, R. M. Suter, and J. F. Nagle, *Biophys. J.* **71**(2), 885 (1996).
- ²²L. K. Nielsen, A. Vishnyakov, K. Jorgensen, T. Bjornholm, and O. G. Mouritsen, *J. Phys.: Condens. Matter* **12**(8A), A309 (2000).
- ²³D. P. Tieleman and H. J. C. Berendsen, *J. Chem. Phys.* **105**(11), 4871 (1996).
- ²⁴J. C. Shillcock and R. Lipowsky, *J. Chem. Phys.* **117**(10), 5048 (2002).
- ²⁵O. G. Mouritsen, A. Boothroyd, R. Harris, N. Jan, T. Lookman, L. MacDonald, D. A. Pink, and M. J. Zuckermann, *J. Chem. Phys.* **79**(4), 2027 (1983).
- ²⁶D. A. Pink, T. J. Green, and D. Chapman, *Biochemistry* **19**(2), 349 (1980).
- ²⁷Z. P. Zhang, M. J. Zuckermann, and O. G. Mouritsen, *Phys. Rev. A* **46**(10), 6707 (1992).
- ²⁸E. Corvera, M. Laradji, and M. J. Zuckermann, *Phys. Rev. E* **47**(1), 696 (1993).
- ²⁹J. H. Ipsen, K. Jorgensen, and O. G. Mouritsen, *Biophys. J.* **58**(5), 1099 (1990).
- ³⁰D. P. Tieleman, S. J. Marrink, and H. J. C. Berendsen, *Biochim. Biophys. Acta* **1331**(3), 235 (1997).
- ³¹M. K. Themis Lazaridis, *Proteins: Struct., Funct., Genet.* **35**(2), 133 (1999).
- ³²M. J. Stevens, *J. Chem. Phys.* **121**(23), 11942 (2004).
- ³³J. C. Shelley, M. Y. Shelley, R. C. Reeder, S. Bandyopadhyay, and M. L. Klein, *J. Phys. Chem. B* **105**(19), 4464 (2001).
- ³⁴S. J. Marrink, H. J. Risselada, S. Yefimov, D. P. Tieleman, and A. H. de Vries, *J. Phys. Chem. B* **111**(27), 7812 (2007).
- ³⁵S. J. Marrink and A. E. Mark, *J. Am. Chem. Soc.* **125**(49), 15233 (2003).
- ³⁶B. J. Reynwar, G. Illya, V. A. Harmandaris, M. M. Muller, K. Kremer, and M. Deserno, *Nature (London)* **447**(7143), 461 (2007).
- ³⁷S. J. Marrink, J. Risselada, and A. E. Mark, *Chem. Phys. Lipids* **135**(2), 223 (2005).
- ³⁸P. B. Warren, *Curr. Opin. Colloid Interface Sci.* **3**(6), 620 (1998).
- ³⁹S. Yamamoto, Y. Maruyama, and S. Hyodo, *J. Chem. Phys.* **116**(13), 5842 (2002).

- ⁴⁰M. Kranenburg, M. Venturoli, and B. Smit, *J. Phys. Chem. B* **107**(41), 11491 (2003).
- ⁴¹G. Brannigan, A. C. Tamboli, and F. L. H. Brown, *J. Chem. Phys.* **121**(7), 3259 (2004).
- ⁴²F. S. Hing and G. G. Shipley, *Biochemistry* **34**(37), 11904 (1995).
- ⁴³J. T. Kim, J. Mattai, and G. G. Shipley, *Biochemistry* **26**(21), 6592 (1987).
- ⁴⁴O. Berger, O. Edholm, and F. Jahnig, *Biophys. J.* **72**(5), 2002 (1997).
- ⁴⁵S. E. Feller and A. D. MacKerell, *J. Phys. Chem. B* **104**(31), 7510 (2000).
- ⁴⁶J. Sonne, M. O. Jensen, F. Y. Hansen, L. Hemmingsen, and G. H. Peters, *Biophys. J.* **92**(12), 4157 (2007).
- ⁴⁷A. D. MacKerell, D. Bashford, M. Bellott, R. L. Dunbrack, J. D. Evanseck, M. J. Field, S. Fischer, J. Gao, H. Guo, S. Ha, D. Joseph-McCarthy, L. Kuchnir, K. Kuczera, F. T. K. Lau, C. Mattos, S. Michnick, T. Ngo, D. T. Nguyen, B. Prodhom, W. E. Reiher, B. Roux, M. Schlenkrich, J. C. Smith, R. Stote, J. Straub, M. Watanabe, J. Wiorkiewicz-Kuczera, D. Yin, and M. Karplus, *J. Phys. Chem. B* **102**(18), 3586 (1998).
- ⁴⁸J. B. Klauda, R. M. Venable, J. A. Freites, J. W. O'Connor, D. J. Tobias, C. Mondragon-Ramirez, I. Vorobyov, A. D. MacKerell, Jr., and R. W. Pastor, *J. Phys. Chem. B* **114**(23), 7830 (2010).
- ⁴⁹C. Anezo, A. H. de Vries, H. D. Holtje, D. P. Tieleman, and S. J. Marrink, *J. Phys. Chem. B* **107**(35), 9424 (2003).
- ⁵⁰H. Heller, M. Schaefer, and K. Schulten, *J. Phys. Chem.* **97**(31), 8343 (1993).
- ⁵¹U. Essmann, L. Perera, and M. L. Berkowitz, *Langmuir* **11**(11), 4519 (1995).
- ⁵²K. Tu, D. J. Tobias, J. K. Blasie, and M. L. Klein, *Biophys. J.* **70**(2), 595 (1996).
- ⁵³R. M. Venable, B. R. Brooks, and R. W. Pastor, *J. Chem. Phys.* **112**(10), 4822 (2000).
- ⁵⁴A. H. de Vries, S. Yefimov, A. E. Mark, and S. J. Marrink, *Proc. Natl. Acad. Sci. U.S.A.* **102**(15), 5392 (2005).
- ⁵⁵W. J. Sun, S. Tristram-Nagle, R. M. Suter, and J. F. Nagle, *Biophys. J.* **70**(2), Wp227 (1996).
- ⁵⁶S. Leekumjorn and A. K. Sum, *Biochim. Biophys. Acta* **1768**(2), 354 (2007).
- ⁵⁷B. Hess, C. Kutzner, D. van der Spoel, and E. Lindahl, *J. Chem. Theory Comput.* **4**(3), 435 (2008).
- ⁵⁸E. Lindahl and O. Edholm, *Biophys. J.* **79**(1), 426 (2000).
- ⁵⁹P. Tieleman (2008); see <http://moose.bio.ucalgary.ca/> for access for download of the files in 2008.
- ⁶⁰S. W. Chiu, M. Clark, V. Balaji, S. Subramaniam, H. L. Scott, and E. Jakobsson, *Biophys. J.* **69**(4), 1230 (1995).
- ⁶¹E. Jürgens, G. Höhne, and E. Sackmann, *Ber. Bunsenges. Phys. Chem.* **87**(2), 95 (1983).
- ⁶²A. W. Schuttelkopf and D. M. F. van Aalten, *Acta Crystallogr., Sect. D: Biol. Crystallogr.* **60**, 1355 (2004).
- ⁶³N. Kucerka, J. F. Nagle, J. N. Sachs, S. E. Feller, J. Pencer, A. Jackson, and J. Katsaras, *Biophys. J.* **95**(5), 2356 (2008).
- ⁶⁴J. P. Douliez, A. Leonard, and E. J. Dufourc, *J. Phys. Chem.* **100**(47), 18450 (1996).
- ⁶⁵M. Picquart and T. Lefèvre, *J. Raman Spectrosc.* **34**(1), 4 (2003).
- ⁶⁶R. Mendelsohn, M. A. Davies, J. W. Brauner, H. F. Schuster, and R. A. Dluhy, *Biochemistry* **28**(22), 8934 (1989).
- ⁶⁷R. N. A. H. Lewis and R. N. McElhaney, *Chem. Phys. Lipids* **96**(1–2), 9 (1998).
- ⁶⁸L. S. Vermeer, B. L. de Groot, V. Reat, A. Milon, and J. Czapllicki, *Eur. Biophys. J.* **36**, 919 (2007).
- ⁶⁹V. A. Raghunathan and J. Katsaras, *Phys. Rev. E* **54**(4), 4446 (1996).
- ⁷⁰S. E. Feller and R. W. Pastor, *Biophys. J.* **71**(3), 1350 (1996).
- ⁷¹J. B. Klauda, N. Kucerka, B. R. Brooks, R. W. Pastor, and J. F. Nagle, *Biophys. J.* **90**(8), 2796 (2006).
- ⁷²J. S. Hub, T. Salditt, M. C. Rheinstader, and B. L. de Groot, *Biophys. J.* **93**(9), 3156 (2007).
- ⁷³K. Kjaer, *Physica B* **198**(1–3), 100 (1994).
- ⁷⁴E. B. Sirota, H. E. King, D. M. Singer, and H. H. Shao, *J. Chem. Phys.* **98**(7), 5809 (1993).
- ⁷⁵J. F. Nagle, *Annu. Rev. Phys. Chem.* **31**, 157 (1980).
- ⁷⁶K. Binder, *Rep. Prog. Phys.* **50**, 783 (1987).
- ⁷⁷H. Ebel, P. Grabitz, and T. Heimburg, *J. Phys. Chem. B* **105**(30), 7353 (2001).
- ⁷⁸H. Kojima, K. Hanada-Yoshikawa, A. Katagiri, and Y. Tamai, *J. Biochem. (Tokyo)* **103**, 126 (1988). See <http://jb.oxfordjournals.org/content/103/1/126.short>.
- ⁷⁹M. Janiak, D. Small, and G. Shipley, *Biochemistry* **15**(21), 4575 (1976).
- ⁸⁰M. Rief, M. Gautel, F. Oesterhelt, J. M. Fernandez, and H. E. Gaub, *Science* **276**(5315), 1109 (1997).
- ⁸¹E. Evans and K. Ritchie, *Biophys. J.* **72**(4), 1541 (1997).
- ⁸²G. I. Bell, *Science* **200**(4342), 618 (1978).
- ⁸³See supplementary material at <http://dx.doi.org/10.1063/1.3615937> for an experimental DSC curve.